Numerical Simulation of a Cryogenic Plant for the Cooling of Mashed Grapes

Raffaele Romano[1], Andrea Formato[1], and Francesco Villecco[2(✉)]

[1] Department of Agricultural Science, University of Naples "Federico II", via Università 100, 80055 Portici, Naples, Italy
[2] Department of Industrial Engineering, University of Salerno, via Giovanni Paolo II 132, 84084 Fisciano, Italy
fvillecco@unisa.it

Abstract. A numerical model of cryo-maceration plant for mashed grapes has been realized to simulate the rapid cooling process for mashed grapes according to the number of nozzles enabled to inject CO_2, to their flow and temperature of CO_2 injected. ANSYS CFX program was used and two geometries have been considered with the axis of each nozzle orthogonal and parallel to the flow direction. Different boundary conditions have been considered. For the models have been considered the most burdensome condition.

Keywords: Numerical simulation · Cryo-maceration plant · Liquid CO_2

1 Introduction

Plants for cryo-maceration to perform rapid cooling of mashed grapes are used to realize adjustable temperature difference DT between 12 and 25 °C with respect to the ambient temperature [1, 2]. These plants [3, 4] have the nozzles that inject liquid CO_2 for the mashed grapes refrigeration [5], and they guarantee an optimal refrigeration process [6, 7]. The plant is composed by: [8] Liquid carbon dioxide injector, Transfer pipeline, Solid-gas separation cyclone. The inlet of the injector is formed by a tube [9] in which the nozzles for injecting carbon snow are inserted [10]. Further, there is a temperature probe, and a pressure switch suitable to detect any malfunctions of the injection system [11]. The transfer piping [12, 13] links the injector to the separation cyclone [14].

2 Research Methodology

The plant, consists of two pipes, both of circular cross-section, connected by a divergent stretch [15]. It is vertically arranged, and the flow of grapes is pressed from bottom to top [16]. The pipe upstream of the divergent has a diameter of 100 mm and is 100 mm long, while that downstream of the divergent has a diameter of 300 mm and is 6 m long [17]. The divergent, consisting of a truncated cone with circular bases, is 300 mm long [18]. Each nozzle has a diameter of 2 mm [19]. To evaluate the heat exchange inside the plant, a numerical model was constructed [20] by the ANSYS CFX code [21, 22].

I. Karabegović (Ed.): NT 2021, LNNS 233, pp. 866–874, 2021.
https://doi.org/10.1007/978-3-030-75275-0_95

3 Results

Since the plant is symmetrical, the numerical modeling concerned only half of the plant [23]. The calculations concerned two geometries. In the first, the axis of each nozzle has been considered, with respect to the flow direction, orthogonal, while, in the second, the axis of the nozzles has been considered parallel to the flow direction [24]. In the case in which the nozzle axis is parallel to the flow, moreover, the calculations were made considering two possible boundary conditions, both for the flow of CO_2, and for the mixture composed of pressed and CO_2, coming out of the larger diameter pipe [25–28]. The analyzed cases, therefore, are three, and have been identified as Case 1, Case 2 and Case 3 and precisely:

- Case 1: nozzles with axis orthogonal to the flow. Results obtained in the case of environmental pressure imposed at the plant outlet and mass flow rate imposed on the CO_2 entering from the nozzles [29].
- Case 2: nozzles with axis parallel to the flow. Results obtained in the case of pressure imposed on the entering CO_2 and mass flow rate of the mixture at the outlet of the plant.
- Case 3: nozzles with axis parallel to the flow. Results obtained in the case of environmental pressure imposed at the plant outlet and mass flow rate imposed on the CO_2 entering from the nozzles.

In the models, the calculations concerned the most serious conditions, that is, with the maximum flow rate, equal to about 3600 kg/h, at an initial temperature, at the entrance of the divergent, of 298 K, while that of the Liquid CO_2, equal to 253 K.

3.1 Case 1

Nozzles with axis orthogonal to the flow of mashed grapes. Results obtained in the case of environmental pressure imposed at the plant outlet and mass flow rate imposed on the CO_2 entering from the nozzles, and we have hypothesized:

- the maximum amount of crushed, equal to about 3600 kg/ h;
- all the nozzles active and delivering, overall, a flow of liquid CO_2 equal to 1/10 of that of the mashed grape, or 360 kg/ h;
- initial temperature of the mashed grape, at the inlet of the divergent, equal to 298 K;
- initial temperature of the liquid CO_2, injected by the nozzles, equal to 253 K;
- relevant expression at the exit of the system.

The boundary conditions outlined above are summarized in the Table 1.

The model consists of n. 60481 elements and 21622 nodes. (Figures 1 and first image of Fig. 2). Figures 2 and 3 show the results of the calculations, in terms of temperature distribution, speed and pressure within the system [30–32].

Table 1. Thermo-fluid dynamic loads and boundary conditions

Location	Boundary conditions
Inlet section (D = 100 mm) Type (inlet)	CO_2 liquid Mass Fraction = 0.0 Component: CO_2 Liquid = Mass Fraction Flow Direction = Normal to Boundary Condition Flow Regime = Subsonic Heat Transfer = Total Temperature Total Temperature = 298 [K] Mass Flow Rate = 0.5 [kg s − 1] Mass And Momentum = Mass Flow Rate Turbulence = Medium Intensity and Eddy Viscosity Ratio
Nozzles (n. 3) Type (inlet)	CO2 liquid Mass Fraction = 1 Component: CO_2 Liquid = Mass Fraction Flow Direction = Normal to Boundary Condition Flow Regime = Subsonic Heat Transfer = Total Temperature Total Temperature = 253 [K] Mass Flow Rate = 0.05 [kg s − 1] Mass And Momentum = Mass Flow Rate Turbulence = Medium Intensity and Eddy Viscosity Ratio
Outlet section (D = 300 mm) Type (outlet)	Flow Regime = Subsonic Mass And Momentum = Average Static Pressure Relative Pressure = 0 [atm] Pressure Averaging = Average Over Whole Outlet
Longitudinal plane of symmetry	
Cloak of the pipes and divergent Type(wall)	Heat Transfer = Adiabatic Wall Influence On Flow = No Slip Wall Roughness = Smooth Wall

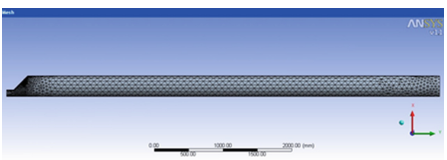

Fig. 1. Overall view of the numerical model of the cooling system.

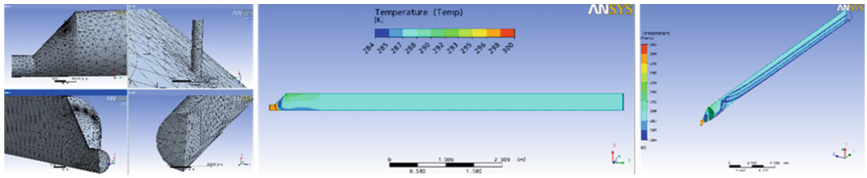

Fig. 2. First: Detailed view of the numerical model. Above: particular Venturi tube (left) and one of the nozzles (right); bottom: plane of symmetry and detail of the inlet section (left) and outlet section (right). Second and third: Temperature field in the symmetry plane of the cooling plant. Overall view of the temperature field in the model considered.

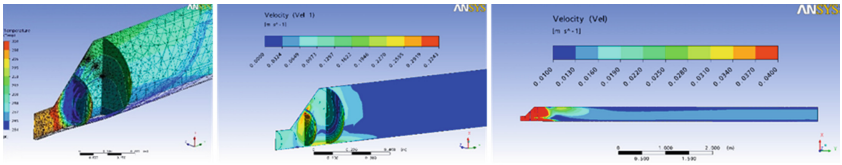

Fig. 3. First: temperature field in the inlet zone of the CO_2 liquid. Second and third: Velocity field. Detail at the divergent.

3.1.1 Temperature, Velocity and Pressure Field

The second image of Fig. 2 shows the temperature trend in the symmetry plane of the cooling system, while in the third image Fig. 2 the same temperature range in an isometric view, in which the liquid CO_2 flow lines are represented. The latter start from the nozzle section, interact, exchanging heat, with the movement field of the mashed grapes, and continue up to the outlet section of the system. The second and third image of Figs. 2 also show that the mashed grapes, at the outlet of the plant, reach a temperature of about 288 K. Figure 3 shows a detail of the same temperature range and of the liquid CO_2 flow lines in the divergent and nozzle areas, and in which the temperature trend is shown, as well as on the symmetry plane, also on two sections transversal of the plant, in order to have a three-dimensional view of the temperature trend [33]. In the divergent portion, having an increase in pressure due to the increase in section of the pipe, the CO_2 flow lines are pushed towards the area under reduced pressure, as is shown in Fig. 3.

In the second and third images of Figs. 3 show the trend of the velocity field. Finally, in Fig. 4, the trend of the pressure field is shown which, similarly to what has been described about the speed range, shows a turbulent zone in the divergent section and a nearly uniform trend in a good part of the crushed outlet line [34]. The same figure shows that the relative pressure inside the pipeline is practically nil, reaching the few tens of Pa.

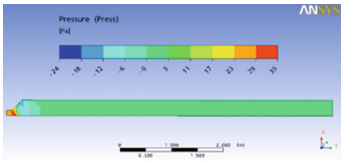

Fig. 4. Pressure field.

3.2 Case 2

Nozzles with axis parallel to the flow of pressed grapes. Results in the case of pressure imposed on the incoming CO_2 and mass flow rate of the mixture at the system outlet. In the second model, the calculations have been made assuming:

- the maximum amount of crushed, equal to about 3600 kg/ h;
- all the active nozzles, and each delivering liquid CO_2 at 20×10^5 Pa;
- initial temperature of the crushed, at the entrance of the divergent, equal to 298 K;
- initial temperature of the liquid CO_2, injected by the nozzles, equal to 253 K.
- Port to the output of the plant equal to 3960 kg/h.

For the details of the mathematical treatment of turbulent phenomena, of the walls of the pipeline and of the symmetry planes, please refer to the previous Table 1. The model consists of n. 17538 elements and 6345 nodes (Fig. 5). Unlike the first model, the axis of each nozzle was considered parallel to the direction of the crushed flow. Furthermore, to lighten the computational burden, only 1/6 of the model has been analyzed, thus assuming a coaxiality between the connected pipes [35].

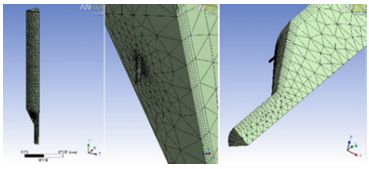

Fig. 5. Overall View of the numerical model.

3.2.1 Temperature, Velocity and Pressure Field

The images of Fig. 6 show the temperature trend in the vertical plane and passing through the nozzle axis. Unlike Case 1, where the flow of CO_2 was orthogonal to that of the pressed, there is no evidence of an area in which the carbon dioxide tends to flow, due to the positive pressure gradient that occurs in the motion, towards the minor section of the divergent. In Third and fourth images of Fig. 6 the trend of the velocity field is shown. Finally, in the fifth image in Fig. 6 shows the trend of the pressure field which, similarly to what observed in the first model, it is possible to see a slight deterioration due to pressure drops.

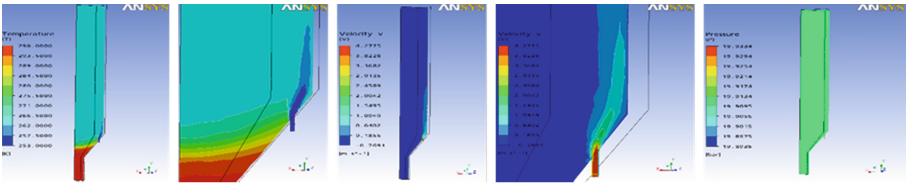

Fig. 6. First and second: temperature trend. On the right A dx, detailed view near the nozzle. Third and fourth: Velocity trend. On the right, detail view near the nozzle. Fifth: pressure field.

3.3 Case 3

Nozzles with axis parallel to the flow of pressed grapes. Results obtained in the case of environmental pressure imposed at the plant outlet and mass flow rate imposed on the CO_2 entering from the nozzles. In the third model we have hypothesized:

- the maximum amount of crushed, equal to about 3600 kg/ h;
- all the nozzles active and delivering, overall, a flow of liquid CO_2 equal to 1/10 of that of the crushed, or 360 kg/ h;
- initial temperature of the crushed, at the entrance of the divergent, equal to 298 K;
- initial temperature of the liquid CO_2, injected by the nozzles, equal to 253 K.
- zero relative pressure at the system outlet.

The numerical model is the one used in Case 2, having only changed the boundary conditions. Figures 7 shows the results of the temperature trend. In this model, the calculations were made assuming the starting hypotheses specified above [36, 37].

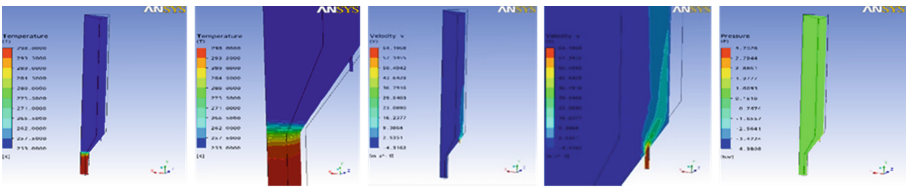

Fig. 7. First and second: Temperature trend. Third and fourth: Velocity trend. In the fourth, detail view near the nozzle. Fifth: the trend of the pressure field.

3.3.1 Temperature, Velocity and Pressure Field

In first and second images of Fig. 7, the temperature trend is shown, passing through the nozzle axis. In Fig. 7 the trend of the velocity field is shown. In the fifth image of Fig. 7 shows the trend of the pressure field which, similarly to what was observed in the other two models, shows a modest reduction due to load losses.

4 Conclusion

Three emblematic cases have been considered for acryomaceration plant: case 1, case 2, case 3, evaluating the pressure and temperature ranges for them. As was to be expected, if a pressure of 20 bar is imposed on the flow entering from the nozzle, and no pressure is imposed on the output equal to the atmospheric one, the whole pipe, including the section of pipe with a smaller diameter, it is attested on this value of the pressure.

However, if the tank pressure is 20 bar, knowing the characteristic of the nozzle, it is possible to know the flow rate supplied by the same as a function of the pressure drop.

References

1. Houbak-Jensen, L., Holten, A., Blarke, M.B., Groll, E.A., Shakouri, A., Yazawa, K.: Dynamic analysis of a dual-mode CO2 heat pump with both hot and cold thermal storage. ASME International Mechanical Engineering Congress and Exposition, Proceedings (IMECE), vol. 8 B (2013)
2. Salvati, L., d'Amore, M., Fiorentino, A., Pellegrino, A., Sena, P, Villecco, F.: Development and testing of a methodology for the assessment of acceptability systems. Machines **8**(47) (2020)
3. Formato, A., Ianniello, D., Romano, R., Pellegrino, A., Villecco, F.: Design and development of a new press for grape marc. Machines **7**(3), 51 (2019)
4. Pappalardo, C.M., Lombardi, N., Dašic´, P.V., Guida, D.: Design and development of a virtual model of an electric vehicle of category L7. In: IOP Conference Series: Materials Science and Engineering, vol. 568, art. no. 012114 (2019)
5. Formato, A., Ianniello, D., Pellegrino, A., Villecco, F.: Vibration-based experimental identification of the elastic moduli using plate specimens of the olive tree. Machines **7**(2), art. no. 46 (2019). https://doi.org/10.3390/machines7020046
6. Naviglio, D., Formato, A., Scaglione, G., Montesano, D., Pellegrino, A., Villecco, F., Gallo, M.: Study of the grape cryo-maceration process at different temperatures. Foods **7**(7), art. no. 107 (2018)
7. Liguori, A., Armentani, E., Bertocco, A., Formato, A., Pellegrino, A., Villecco, F.: Noise reduction in spur gear systems. Entropy **22**, 1306 (2020)
8. Villecco, F., Aquino, R.P., Calabrò, V., Corrente, M.I., Grasso, A., Naddeo,V.: Fuzzy-assisted ultrafiltration of wastewater from milk industries. In: Naddeo, V., Balakrishnan, M., Choo, KH., (eds.), Frontiers in Water-Energy-Nexus—Nature-Based Solutions, pp. 239–242. Springer: Cham, Swiss (2020)
9. Salvati, L., d'Amore, M., Fiorentino, A., Pellegrino, A., Sena, P., Villecco, F.: On-road detection of driver fatigue and drowsiness during medium-distance journeys. Entropy **23**(2), 135 (2021)
10. Sarkar, J., Bhattacharyya, S., Gopal, M.R.: Simulation of a transcritical CO_2 heat pump cycle for simultaneous cooling and heating applications. Int. J. Refrig **29**(5), 735–743 (2006)
11. De Simone, M.C., Guida, D.: Modal coupling in presence of dry friction. Machines **6**(1), 8 (2018). https://doi.org/10.3390/machines6010008
12. Formato, G., Romano, R., Formato, A., Sorvari, J., Koiranen, T., Pellegrino, A., Villecco, F.: Fluid-structure interaction modeling applied to peristaltic pump flow simulations. Machines **7**(3), art. no. 50 (2019)
13. Guida, R., De Simone, M.C., Dašic´, P., Guida, D.: Modeling techniques for kinematic analysis of a six-axis robotic arm. IOP Conf. Ser.: Mater. Sci. Eng. **568**(1), 012115 (2019)

14. Llopis, R., Cabello, R., Sánchez, D., Torrella, E.: Energy improvements of CO_2 transcritical refrigeration cycles using dedicated mechanical subcooling. Int. J. Refrig **55**, 129–141 (2015)
15. Shao, L.L., Zhang, C.L.: Thermodynamic transition from subcritical to transcritical CO_2 cycle. Int. J. Refrig **64**, 123–129 (2016)
16. De Simone, M.C., Rivera, Z.B., Guida, D.: (2018) Obstacle avoidance system for unmanned ground vehicles by using ultrasonic sensors. Machines **6**(2), art. no. 18 (2018). https://doi.org/10.3390/machines6020018
17. Celenta, G., De Simone, M.C.: Retrofitting techniques for agricultural machines. Lect. Notes Netw. Syst. **128** LNNS, 388–396 (2020)
18. Ullrich, B., Wang, J.: Optical properties of PbS quantum dots deposited on glass employing a supercritical CO_2 fluid process. Appl. Sci. **9**, art. no. 467 (2019)
19. Rivera, Z.B., De Simone, M.C., Guida, D.: Unmanned ground vehicle modelling in Gazebo/ROS-based environments. Machines **7**, art. no. 42 (2019)
20. Pappalardo, C.M., Guida, D.: On the computational methods for solving the differential-algebraic equations of motion of multibody systems. Machines **6**(2), art. no. 20 (2018). https://doi.org/10.3390/machines6020020
21. Pappalardo, C.M., Guida, D.: System identification algorithm for computing the modal parameters of linear mechanical systems. Machines **6**(2), art. no. 12 (2018). https://doi.org/10.3390/machines6020012
22. Guida, D.: Dry friction influence on mechanical system dynamics, Lecture Notes in Networks and Systems (in press)
23. Capone, G., D'Agostino, V., Valle, S.D., Guida, D.: Influence of the variation between static and kinetic friction on stick-slip instability. Wear **161**(1–2), 121–126 (1993)
24. Karabegović, I., Karabegović, E., Mahmić, M., Husak, E.: Dissemination of patents of the base technologies of the fourth industrial revolution. Lect. Notes Netw. Syst. **128**, 3-15 (2020)
25. Sicilia, M., De Simone, M.C.: Development of an energy recovery device based on the dynamics of a semi-trailer. Lect. Notes Mech. Eng. 74–84 (2020). https://doi.org/10.1007/978-3-030-50491-5_8
26. Han, J., Song, Y., Tang, W., Wang, C., Fang, L., Zhu, H., Zhao, J., Sun, J.: Reveal the deformation mechanism of (110) silicon from cryogenic temperature to elevated temperature by molecular dynamics simulation. Nanomaterials **9**(11), 1632 (2019)
27. Hackenschmidt, R., Alber-Laukant, B., Rieg, F.: Simulating nonlinear materials under centrifugal forces by using intelligent cross-linked simulations. Strojniškivestnik J. Mech. Eng. **57**, 531–538 (2010)
28. Pappalardo, C.M., Guida, D.: On the dynamics and control of under actuated nonholonomic mechanical systems and applications to mobile robots. Arch. Appl. Mech. **89**(4), 669–698 (2019)
29. Formato, A., Guida, D., Ianniello, D., Villecco, F., Lenza, T.L., Pellegrino, A.: Design of delivery valve for hydraulic pumps. Machines **6**(44) (2018)
30. Karabegović, I., Turmanidze, R., Dašić, P.: Global trend of implementation of industrial robots relating to industry 4.0. Lect. Notes Mech. Eng. 147–155 (2020). https://doi.org/10.1007/978-3-030-50794-7_15
31. Nezirić, E., Isić, S., Karabegović, I., Voloder, A.: FEM model of misaligned rotational system with rotating looseness. Lect. Notes Netw. Syst. **42**, 135–143 (2019). https://doi.org/10.1007/978-3-319-90893-9_16
32. Karabegović, I., Turmanidze, R., Dašić, P.: Robotics and automation as a foundation of the fourth industrial revolution-industry 4.0. Lect. Notes Mech. Eng. 128–136 (2020). https://doi.org/10.1007/978-3-030-40724-7_13
33. JovanovicDolecek, G., Karabegović, I.: Green technology approach to comb-based decimators design. Lect. Notes Netw. Syst. **128**, 469–477 (2020). https://doi.org/10.1007/978-3-030-46817-0_54

34. Capone, G., D'Agostino, V., Valle, S.D., Guida, D.: Stick-slip instabilityanalysis. Meccanica **27**(2), 111–118 (1992)
35. Capone, G., D'Agostino, V., Guida, D.: A finite length plain journal bearing theory. J. Tribol. **116**(3), 648–653 (1994)
36. Pappalardo, C.M.: A natural absolute coordinate formulation for the kinematic and dynamic analysis of rigid multibody systems. Nonlinear Dyn. **81**(4), 1841–1869 (2015). https://doi.org/10.1007/s11071-015-2111-4
37. Li, T., Kou, Z., Wu, J., Yahya, W., Villecco, F.: Vibrational and Acoustical Methods for Structural Health Monitoring. Shock. Vibr. **2021**, art. no. 6614633 (2021)